HOKKAIDO UNIVERSITY

Title	Water Gas Shift Reaction and Effect of Gasification Reaction in Packed-bed under Heating-up Condition
Author(s)	Kashiwaya, Yoshiaki; Ishii, Kuniyoshi
Citation	ISIJ International, 59(4), 643-654 https://doi.org/10.2355/isijinternational.ISIJINT-2018-470
Issue Date	2019-04-15
Doc URL	http://hdl.handle.net/2115/75673
Rights	著作権は日本鉄鋼協会にある
Type	article
File Information	ISIJ Int. 59(4)_ 643-654 (2019).pdf

Instructions for use

Hokkaido University Collection of Scholarly and Academic Papers : HUSCAP

ISIJ International, Vol. 59 (2019), No. 4, pp. 643–654

Water Gas Shift Reaction and Effect of Gasification Reaction in Packed-bed under Heating-up Condition

Yoshiaki KASHIWAYA[1)]* and Kuniyoshi ISHII[2)]

1) Dept. of Energy Science and Technology, Kyoto University, Yoshida Honmachi, Sakyo-ku, Kyoto, 606-8501 Japan.
2) Prof. Emeritus, Hokkaido University. Passed away in 2017.

(*Received on July 2, 2018; accepted on September 27, 2018*)

For the decrease of CO_2 emission from ironmaking field, it is important to clarify the behaviors of hydrogen in blast furnace (BF). However, when hydrogen content increased in BF, many reactions related to hydrogen occurred, and many complicated relationships among the reactions are generated. Especially, the behavior of water gas shift reaction (WGSR) is not understood correctly and the effects on the gasification reaction and the reduction reaction are not known at all.

In the present study, the interest was focused on the relationship between WGSR and coke gasification reaction. The WGSR was examined experimentally and kinetic analysis was performed with and without gasification reaction. The quantification of reaction rates was carried out by gas analysis method. Several kind of crucibles were developed for determining the respective reaction rates occurring in different position.

The rate equation of invers WGSR was decided as

$$R_{sh-i} = -\frac{dCO_2}{dt} = +\frac{dH_2O}{dt} = r_{H2O}\left(\frac{mol}{s\cdot cm^3-bed}\right) = Ak_{sh-i}\left(C_{CO2}C_{H2} - C^e_{CO2}C^e_{H2}\right)$$

where the rate constant in the alumina crucible was obtained as

$$k'_{sh-i}\left(\frac{cm^3-bed}{s\cdot mol}\right) = 107\times10^{+9}\exp\left(\frac{-117\,430}{RT}\right)$$

The single WGSR in alumina crucible is in an equilibrium state over 1 573 K. Calculation of gasification reaction (K_B, Boudouard reaction) in Zone 1 and Zone 1+2+3 were in excellent agreement with the observation under CO–CO_2 system (without Hydrogen). When H_2 was added to the reaction gases, Water gas reaction I (K_{W1}) and II (K_{W2}) in addition to K_B were calculated separately and the total gasification reaction RCS_{cal} ($=K_B+K_{W1}+K_{W2}$) was in good agreement with the observation. The relationship between the separated gasification reactions (K_B, K_{W1} and K_{W2}) and WGSR was discussed.

KEY WORDS: water gas shift reaction; coke gasification; kinetic analysis; rate equation; water gas reaction; Boudouard reaction.

1. Introduction

The authors have investigated the reduction behaviors of iron ores (Pellet and Sinter) using heating-up condition.[1,2)] In these experiments, a basic sinter was used, which was grinded into a sphere as same as the pellet. The sinter was put between two coke layers in order to simulate the conditions in the blast furnace (BF). Since the crucible was made of graphite, the effect of gasification reaction of graphite could not be ignored in the high temperature region.

Recently, a utilization of hydrogen or hydrogen bearing substance (CH_4) in the BF was increasing in order to decrease the CO_2 emission. When the hydrogen was introduced into BF process, the kind of reactions extremely increases in addition to CO reduction (Eq. (1)) and Boudouard reaction (= coke gasification reaction or coke solution loss reaction) (Eq. (3)). In addition to hydrogen reduction (Eq. (2)), water gas reactions (Eqs. (4) and (5)) play an important role. Furthermore, the behavior of water gas shift reaction (WGSR, Eq. (6)) is not yet understanding clearly, because WGSR proceeds both side and depends on the condition of reaction gases and the nature of solid surface (kind of catalysis). Consequently, the following reactions must be taken into account for the analysis of the reaction system, when hydrogen was introduced.

In Eqs. (1) and (2), Fe_xO_y and Fe_xO_{y-1} mean a step of reduction in the series of reductions ($Fe_2O_3\rightarrow Fe_3O_4\rightarrow Fe_xO\rightarrow Fe$), respectively.

Reduction reaction by CO gas (Red-CO):

$$Fe_xO_y + CO \leftrightarrows Fe_xO_{y-1} + CO_2, \quad \Delta H^o = -2.1\ \text{kcal / CO-mol},$$

$$K_{CO} = \frac{P^e_{CO2}}{P^e_{CO}} \qquad \text{..... (1)}$$

Reduction reaction by H_2 gas (Red-H_2):

$$Fe_xO_y + H_2 \leftrightarrows Fe_xO_{y-1} + H_2O, \quad \Delta H^o = +7.8\ \text{kcal / } H_2\text{-mol},$$

$$K_{H2} = \frac{P^e_{H2O}}{P^e_{H2}} \qquad \text{.. (2)}$$

* Corresponding author: E-mail: Kashiwaya@energy.kyoto-u.ac.jp
DOI: https://doi.org/10.2355/isijinternational.ISIJINT-2018-470

© 2019 ISIJ

Boudouard reaction (BR):

$$C + CO_2 \leftrightarrows 2CO, \qquad \Delta H^o = +41 \text{ kcal / C-mol}, \qquad K_{BD} = \frac{P_{CO}^{e\,2}}{P_{CO2}^e} \quad \text{..... (3)}$$

Water gas reaction I (WGRI)

$$C + H_2O \leftrightarrows H_2 + CO, \qquad \Delta H^o = +31 \text{ kcal / C-mol}, \qquad K_{WG} = \frac{P_{H2}^e P_{CO}^e}{P_{H2O}} \quad \text{..... (4)}$$

Water gas reaction II (WGRII):

$$C + 2H_2O \leftrightarrows 2H_2 + CO_2, \quad \Delta H^o = +21 \text{ kcal / C-mol}, \qquad K_{WG2} = \frac{P_{H2}^{e\,2} P_{CO2}^e}{P_{H2O}^{e\,2}} \quad \text{..... (5)}$$

Water gas shift reaction (WGSR):

$$H_2O + CO \leftrightarrows H_2 + CO_2, \quad \Delta H^o = -9.8 \text{ kcal / } H_2\text{-mol}, \qquad K_{Sh} = \frac{P_{H2}^e P_{CO2}^e}{P_{H2O}^e P_{CO}^e} \quad \text{... (6)}$$

It is generally considered that the hydrogen reduction has a disadvantage because of endothermic reaction (Eq. (2), ΔH^o=+7.8 kcal/H_2-mol). However, if the hydrogen reduction (Eq. (2)) occurred, the WGSR (Eq. (6), ΔH^o=−9.8 kcal/H_2-mol) should occur together. The overall reaction would be the same as the CO reduction (Eq. (1), ΔH^o=−2.1 kcal/CO-mol) which is the exothermic reaction.

The same relationship can be applied to the water gas reactions (Eqs. (4) and (5)) and WGSR (Eq. (6)), and those reactions compose a Boudouard reaction (Eq. (3)), apparently.

From these consideration, the behavior of WGSR is important for understanding the system containing H_2 gas.

However, the WGSR actually proceeds opposite direction, which is called as the inverse water gas shift reaction (i-WGSR, Eq. (6')) in the present experimental condition.

Inverse Water gas shift reaction (i-WGSR):

$$H_2 + CO_2 \rightleftarrows H_2O + CO \qquad K_{Sh-i} = \frac{P_{H2O}^e P_{CO}^e}{P_{H2}^e P_{CO2}^e} \quad \text{.....(6')}$$

For the sake of convenience, i-WGSR is described as WGSR in later section.

Kashiwaya[1,3] has shown the benefit of reduction by pure hydrogen, in which the rate of reduction is faster than that of CO reduction and the clean iron can be obtained. Before usage of pure hydrogen, we should understand the reactions in CO–CO_2–H_2–H_2O system.

In this study, (a) the reaction kinetics of WGSR occurring in an alumina crucible was clarified, then, (b) the gasification reaction was analyzed and separated into three kinds of reactions (Eqs. (3), (4) and (5)), finally, (c) the behavior of WGSR in the presence of gasification reactions was analyzed and the characteristics of reaction behavior was elucidated.

2. Experimental

Experiments were carried out using Softening-Smelting-Dripping Reduction (SSDR) system (**Fig. 1**) under heating up condition (10 K/min). The detail of experiment has been reported in the previous papers.[1,2,4,5] Total flowrate of reaction gas is 2 000 cm^3(STP)/min and the linear velocity is about 11 cm/s. The base composition of reaction gas is Ar-30 vol%CO. When H_2 and/or CO_2 are/is added, the content of reaction gas is fixed to 30 vol%. When CO_2 is added to the reaction gas, the ratios of CO/CO_2 were fixed to 9/1 and 8/2. Then, the gas compositions were Ar-27.0 vol%CO-3.0 vol%CO_2 for 9/1 and Ar-24.0 vol%CO-6.0 vol%CO_2 for 8/2 (**Table 1**). When hydrogen is added to the reaction gas, the content of hydrogen was basically 3.5 vol% and the rest of reaction gas (26.5 vol%) was adjusted to 9/1 or 8/2 in the ratio of CO/CO_2. However in this experiment, in order to carried out the kinetic analysis of WGSR, hydrogen content in reaction gas increased to 7.0 vol% and the rest of reaction gas (23 vol%) was adjusted to 9/1 and 8/2 in CO/CO_2 ratio, as shown in Table 1. The chemical composi-

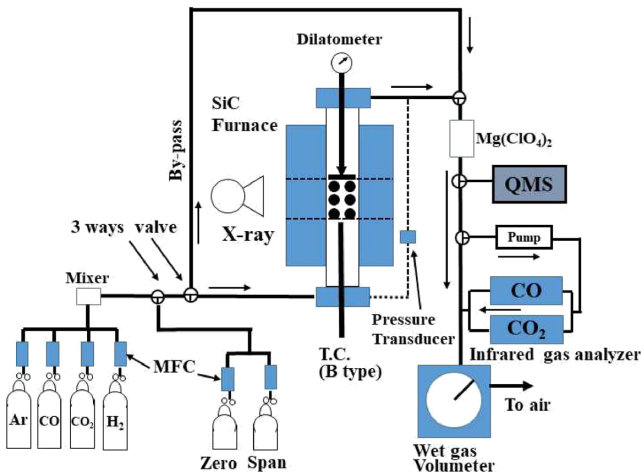

Fig. 1. Heating up reduction setup named the softening-melting-dripping reduction (SMDR) system under loading condition. (Online version in color.)

Table 1. Experimental and calculation conditions.

No.	Sign	Zone	CO In %	CO_2 In %	H_2 In %	Coke	Ore	Crucible	Calculation: Coke+Graphite weight	Bed number	WGS	Gashi. Coke+Gra. (by CO_2)	Gashi. Coke+Gra. (by H_2O)	Red. (by CO)	Red. (by H_2O)
1	Sh-8/2-7	1+2+3	18.4	4.6	7	0	0	Al.	0	80	○	×	×	×	×
2	Z1-9/1-0	1	27.0	3.0	0	2	0	Gra.	10	34	×	○	×	×	×
3	Z1-8/2-0	1	24.0	6.0	0	2	0	Gra.	10	34	×	○	×	×	×
4	Z2-9/1-0	1+2+3	27.0	3.0	0	3	0	Gra.	20	80	×	○	×	×	×
5	Z2-8/2-0	1+2+3	24.0	6.0	0	3	0	Gra.	20	80	×	○	×	×	×
6	Z1-8/2-7	1	18.4	4.6	7	2	0	Gra.	20	34	○	○	○	×	×
7	Z2-8/2-7	1+2+3	18.4	4.6	7	3	0	Gra.	20	80	○	○	○	×	×

Ar+30%(CO+CO_2+H_2), Total Flow rate=2 000 cm^3 (STP)/min
WGS: water gas shift (reaction), Gashi.: Gasification
Gra.: graphite, Al.: Alumina, Red.: Reduction

© 2019 ISIJ

tions of sinter and coke used are summarized in **Table 2**.

2.1. Crucibles Served for Experiments

In this study, the fixed bed analysis was performed, in which the change of gas composition and reaction degree of iron ore and coke gasification in the bed were taken into account.

At first, the rate of WGSR (i-WGSR) was obtained using alumina crucible in which neither of gasification reactions (BR, WGRI and WGRII) nor reduction reactions (Red-CO and Red-H_2) occurred. Second, the gasification reaction (BR) without WGSR was analyzed in the fixed bed system. Finally, the behavior of WGSR occurring with coke gasification was analyzed under hydrogen addition. The analysis of reduction reaction will be presented in the following paper.

In this paper, the relationship between WGSR and coke gasification reaction is focused on. Although the reduction reaction is not covered in this paper, overall image of reactions occurring in the present system is shown as **Fig. 2**.

In the series of this study, the reaction behaviors of burdens (iron ore and coke) in BF were investigated and the process variables were simulated using SSDR.[1,2,4,5] In this experiment, a graphite crucible was used as mentioned above. The bed of iron ore consisting of six spheres was sandwiched between the upper and lower coke beds. The reaction regions in the crucible were classified into three zones and were named as Zone 1, Zone 2 and Zone 3 as shown in Fig. 2.

The inlet gas (reaction gas) reacts with coke and graphite crucible in the lower part (Zone 1) before the reduction reaction occurs, when CO_2 gas was contained. When hydrogen is contained, reactions (Eqs. (3), (4), (5) and (6)) will occur and the gas composition will be changed before reduction reactions occur.

In Zone 2, the reduction reactions (Eqs. (1) and (2): Red-CO and Red-H_2) mainly occur in the bed of iron ore. In addition, gasification reactions (Eqs. (3), (4) and (5)) at the inner surface of graphite crucible occur. The WGSR (Eq. (6)) occurs simultaneously both with reduction reactions and gasification reactions. Finally, in Zone 3, gasification reactions and WGSR occur.

Final destination is to clarify the reaction behaviors in a mixed bed of iron ore and coke in CO–CO_2–H_2–H_2O system (**Fig. 3**(a)). In order to clarify the reactions in Zone 1, crucible was modified as shown in Fig. 3(b). Only the lower coke bed was remained, and the inner surface of graphite crucible was prevented from the gasification reaction by inserting the alumina tube to Zone 2 and Zone 3. The gasification reactions in Zones 1+2+3 were clarified using Fig. 3(c), in which the gasification reaction at the surface of graphite crucible in Zone 2 and the gasification reactions of upper coke and the surface of graphite crucible in Zone 3 were clarified in addition to Zone 1.

As a result, the gasification in Zone 1 and Zones 2+3 were able to estimate separately. Since the WGSR without gasification reactions and reduction reactions must be clarified, reaction bed made of alumina with the same structure as Fig. 3(a) was constructed as shown in **Fig. 4**. In this case, it is considered that the reaction surface and gas flow will strongly affect on WGSR, the structure was arranged as same as possible.

Table 2. Chemical composition of sinter and coke used (mass%).

	T.Fe	FeO	SiO_2	Al_2O_3	CaO	MgO	S	C/S	Fixed C
Sinter	58.7	5.32	5.7	1.92	7.78	1.1	–	1.38	–
Coke	1.1	–	6.0	3.3	0.3	0.2	0.7	0.05	87.5

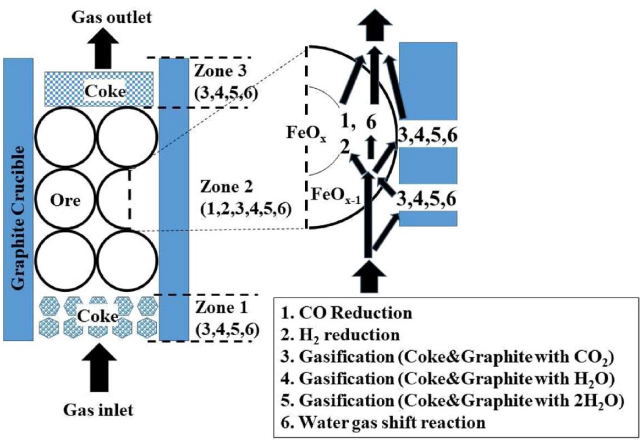

Fig. 2. Reaction system in the present experiment. (Online version in color.)

3. Method of Analysis

The above mentioned reactions from Eq. (1) to Eq. (6) were considered for analysis. In the present study, especially, gasification reactions for coke and graphite (Eqs. (3-a), (3'-a), (4-a), (4'-a), (5-a) and (5'-a)) were separately assessed as shown in Fig. 2. The details of equation of gasification were described in the later section.

$$Fe_xO_y + CO = Fe_xO_{y-1} + CO_2 \quad : R_{CO}\ (\mathrm{mol/s/cm^3-bed}) \qquad \text{(1-a)}$$

$$Fe_xO_y + H_2 = Fe_xO_{y-1} + H_2O \quad : R_{H2}\ (\mathrm{mol/s/cm^3-bed}) \qquad \text{(2-a)}$$

$$C(\mathrm{coke}) + CO_2 = 2CO \quad : R_{BC}\ (\mathrm{mol/s/cm^3-bed}) \qquad \text{(3-a)}$$

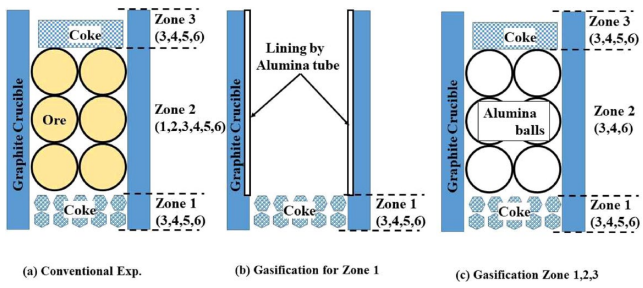

Fig. 3. Structures of crucible for analyzing the behavior of gasification and WGSR. (Online version in color.)

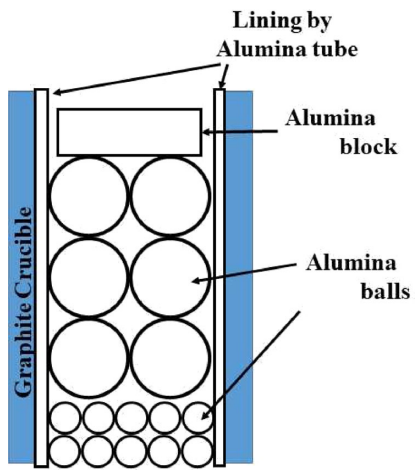

Fig. 4. Structure of crucible for analyzing the behavior of water gas shift reaction (WGSR). (Online version in color.)

© 2019 ISIJ

$$C(graphite) + CO_2 = 2CO \quad : R_{BG}\ (mol/s/cm^3 - bed) \quad \text{.....(3'-a)}$$

$$C(coke) + H_2O = CO + H_2 \quad : R_{WC}\ (mol/s/cm^3 - bed) \quad \text{.....(4-a)}$$

$$C(graphite) + H_2O = CO + H_2 \quad : R_{WG}\ (mol/s/cm^3 - bed) \quad \text{.....(4'-a)}$$

$$C(coke) + 2H_2O = CO_2 + 2H_2 \quad : R_{W2C}\ (mol/s/cm^3 - bed) \quad \text{.....(5-a)}$$

$$C(graphite) + 2H_2O = CO_2 + 2H_2 \quad : R_{W2G}\ (mol/s/cm^3 - bed) \quad \text{.....(5'-a)}$$

$$H_2 + CO_2 = CO + H_2O \quad : R_{sh-i}\ (mol/s/cm^3 - bed) \quad \text{.....(6'-a)}$$

$$R_B = R_{BC} + R_{BG} \quad \text{.....(7)}$$

$$R_W = R_{WC} + R_{WG} \quad \text{.....(8)}$$

$$R_{W2} = R_{W2C} + R_{W2G} \quad \text{.....(9)}$$

The rates of reactions are expressed as R_x (mol/s/cm^3-bed) where the subscript 'x' means the kind of reactions. The subscripts 'CO' and 'H2' mean the CO and H_2 reductions, respectively. 'BC' and 'BG' mean the Boudouard reaction corresponding to coke and graphite, respectively. Total Boudouard reaction R_B consist of R_{BC} and R_{BG} (Eq. (7)). Similarly, total Water gas reaction I, R_W consist of R_{WC} and R_{WG} (Eq. (8)), and Water gas reaction II, R_{W2} consist of R_{W2C} and R_{W2G} (Eq. (9)). On the other hand, Water gas sift reaction (WGSR) is considered as an inverse WGSR which is expressed as R_{sh-i}.

Fixed bed analysis was performed considering a change of gas composition in a bed, where $[CO]_x$, $[CO_2]_x$, $[H_2]_x$, $[H_2O]_x$ are the flow rates of respective gases in cm^3(STP)/min, where the subscript means the step at n or n+1, while 'in' and 'out' mean the inlet and outlet of crucible, respectively (**Fig. 5**).

In a differential section, mass balances in gas phase, and oxygen and carbon balances in solid phase are expressed as follows:

Mass balance in gas phases;

$$u\left(\frac{\partial C_{H2}}{\partial Z}\right) + \varepsilon\left(\frac{\partial C_{H2}}{\partial t}\right) = \left(-R_{H2} + R_W + 2R_{W2} - R_{sh-i}\right) \quad \text{... (10)}$$

$$u\left(\frac{\partial C_{H2O}}{\partial Z}\right) + \varepsilon\left(\frac{\partial C_{H2O}}{\partial t}\right) = \left(R_{H2} - R_W - 2R_{W2} + R_{sh-i}\right) \quad \text{... (11)}$$

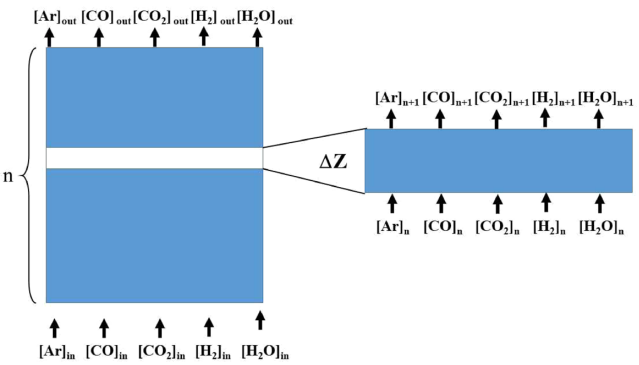

Fig. 5. Illustration of mass balances of oxygen and carbon in the fixed bed analysis. (Online version in color.)

$$u\left(\frac{\partial C_{CO}}{\partial Z}\right) + \varepsilon\left(\frac{\partial C_{CO}}{\partial t}\right) = \left(-R_{CO} + 2R_B + R_W + R_{sh-i}\right) \quad \text{..... (12)}$$

$$u\left(\frac{\partial C_{CO2}}{\partial Z}\right) + \varepsilon\left(\frac{\partial C_{CO2}}{\partial t}\right) = \left(R_{CO} - R_B + R_{W2} - R_{sh-i}\right) \quad \text{..... (13)}$$

Mass balance in solid phase:

Oxygen balance;

$$\frac{\partial F}{\partial t} = (R_{CO} + R_{H2}) \cdot 16 / Wo \quad \text{..... (14)}$$

Carbon balance;

$$\frac{\partial G}{\partial t} = (R_B + R_W + R_{W2}) \cdot 12 \quad \text{..... (15)}$$

The variables used are summarized in the Nomenclature.

The observed gasification rate (RCS(g-C/min), Eq. (16)) and reduction rate (RDR(g-O/min), Eq. (17)) are obtained from gas flow rates, $[CO]_{in}$, $[CO_2]_{in}$, $[H_2O]_{in}$, $[CO]_{out}$, $[CO_2]_{out}$, $[H_2O]_{out}$ in cm^3(STP)/min, where the subscript 'in' means the inlet gas and 'out' means the outlet gas, although the reduction reaction is zero (RDR = 0) in this report.

Gasification rate;

$$RCS(g\text{-}C/min) = \left([CO]_{out} + [CO_2]_{out} - [CO]_{in} - [CO_2]_{in}\right) * 12/22\,414 \quad \text{..... (16)}$$

Reduction rate:

$$RDR(g\text{-}O/min) = \left([CO]_{out} + 2[CO_2]_{out} + [H_2O]_{out} - [CO]_{in} - 2[CO_2]_{in} - [H_2O]_{in}\right) * 16/22\,414 \quad \text{..... (17)}$$

The RDR(g-O/min) can be converted into a percentage RDR(%/min) with an initial reducible oxygen $[O]_o$ (g).

$$RDR(\%/min) = RDR(g\text{-}O/min)/[O]_o \times 100 \quad \text{..... (18)}$$

The calculated reaction rates are as follows;

$$RCS_{cal}(mg\text{-}C/min) = \sum_1^{N_B}\left((R_B + R_W + R_{W2})V_B\right) \times 60 \times 12 \times 1\,000 \quad \text{..... (19)}$$

$$RDR_{cal}(\%/min) = \sum_1^{N_B}\left((R_{CO} + R_{H2})V_B\right) \times 60 \times 16/[O]_o \times 100 \quad \text{..... (20)}$$

3.1. Determination of Rate Equation of WGSR

3.1.1. Comparison with the Equations Reported by other Researchers

Kinetic analysis has been performed by many researchers. Especially, in the production of synthesis gas, WGSR is important reaction. Many kinds of catalyst were developed and reported on the rate of WGSR.[6] In addition, several reviews[7,8] were reported on the WGSR. However, the WGSR in BF, when the hydrogen content increased, is quite different from the production of synthesis gas. In the case of BF, carbon and oxygen in solid phase move to gas phase thorough gasification reaction and reduction reaction, which means that the mass balances of carbon and oxygen always changes in gas phase. The changes on the mass balance must be taken into account on the kinetic analysis.

Unfortunately, there is little study on the WGSR considering the both circumstances of reduction reaction and gasification reaction. A. Kemppainen, *et al.*[9] reported the behavior of WGSR in the packed bed of Olivine pellet.

© 2019 ISIJ

T. Murayama, *et al.*[10] studied the WGSR in the wustite packed bed and presented a rate equation (Eq. (21)).

$$Rw\left(\frac{mol}{s\cdot m^3-bed}\right) = \frac{4}{3}\pi r_0^3 N_p k_w' P^2\left(K_W X_{CO} X_{H2O} - X_{CO2} X_{H2}\right)F \quad \text{..... (21)}$$

where r_0 is radius of pellet (m), Np is number of pellet per volume in bed (Particles/m^3-bed), k'_w is rate constant of inverse WGSR (mol/s m^3 Pa^2), P is total pressure (Pa) and Xj is mole fraction of j element. K_W ($=P_{CO2}P_{H2}/P_{CO}P_{H2O}$) is equilibrium constant of WGSR. F is reduction degree and assumed to be unity in this study.

For the sake of comparison with other researcher's results, the Eq. (21) was transformed into Eq. (22). Then, term of $\beta_1 \cdot k'_w$ was compared with other researchers.

$$Rw\left(\frac{mol}{s\cdot cm^3-bed}\right) = \frac{4}{3}\pi r_0^3 N_p\left(1\times10^{-6}\right)\left(101\,325\right)^2 Fk_w'\left(P_{CO2}P_{H2} - P_{CO}P_{H2O}\cdot K_W\right) = \beta_1\cdot k_w'\left(P_{CO2}P_{H2} - P_{CO}P_{H2O}\cdot K_W\right) \quad \text{... (22)}$$

The rate constant k'_w is given by Eq. (23) and the activation energy is about 52 kJ.

$$k_w'\left(\frac{mol}{s\cdot m^3 Pa^2}\right) = 3.76\times10^{-4}\exp\left(\frac{-52\,460}{RT}\right) \quad \text{..... (23)}$$

M. Ishigaki, *et al.*[11] has presented Eq. (24) for WGSR in a shaft furnace with iron oxide pellet.

$$-\frac{dCO_2}{dt}\left(\frac{mol}{s\cdot cm^3-bed}\right) = V_p k_w\left(P_{CO2}P_{H2} - P_{CO}P_{H2O}\cdot K_W\right) \quad \text{.. (24)}$$

Equation (24) was also transformed into Eq. (25).

$$= \beta_2\cdot k_w'\left(P_{CO2}P_{H2} - P_{CO}P_{H2O}\cdot K_W\right) \quad \text{..... (25)}$$

The rate constant $k_w'(Fe)$ is given by Eq. (26) and the activation energy is about 32 kJ.

$$k_w'(Fe)\left(\frac{mol}{s\cdot cm^3 atm^2}\right) = 1.355\times10^{-2}\exp\left(\frac{-32\,400}{RT}\right) \quad \text{.... (26)}$$

Grabke, *et al.*[12] has presented Eq. (27) which considered the activity of oxygen in iron oxide.

$$n_{CO}/A\left(\frac{mol}{s\cdot cm^2}\right) = k'\left[a_O\right]\left(P_{CO2} - a_O P_{CO}\right) \quad \text{..... (27)}$$

where $[a_o]$ is an activity of iron oxide (Eq. (28)) and k_O is a rate constant (Eq. (29)) in which the activation energy is about 124 kJ. For the Garabke's equation, the surface area was assumed as 3 000 cm^2 for the comparison which is mentioned later.

$$k'\left[a_O\right] = k_O\cdot a_O^{-m},\left(m=\frac{2}{3}, at\ 900°C\right) \quad \text{..... (28)}$$

$$k_O\left(\frac{mol}{s\cdot cm^3 atm}\right) = 0.00717\exp\left(\frac{-124\,700}{RT}\right) \quad \text{..... (29)}$$

3.1.2. Rate Equation in the Present Study

Rate equation of water gas shift reaction WGSR in the present study is shown in Eq. (30).

On the basis of above mentioned references,[6–12] the rate equation is defined as the product of 'surface area', 'rate constant' and 'driving force'.

$$R_{sh-i} = -\frac{dCO_2}{dt} = +\frac{dH_2O}{dt} = r_{H2O}\left(\frac{mol}{s\cdot cm^3-bed}\right) \quad \text{... (30)}$$

$$= Ak_{sh-i}\left(C_{CO2}C_{H2} - C_{CO2}^e C_{H2}^e\right)$$

$$= Ak_{sh-i}\left(P_{CO2}P_{H2} - P_{CO2}^e P_{H2}^e\right)/\left(RT\right)^2 \quad \text{..... (31)}$$

In order to compare with the other researcher's results, the term of driving force was remained, and the other terms were put into two terms ($\alpha\cdot k'_{sh-i}$, Eq. (32)).

$$= \alpha\cdot k_{sh-i}'\left(P_{CO2}P_{H2} - P_{CO2}^e P_{H2}^e\right) \quad \text{..... (32)}$$

where $k'_{sh-i} = Ak_{sh-i}$ and $\alpha = 1/(RT)^2$.

The apparent rate constant, k'_{sh-i} in present experiment was obtained using results of experiment (sh-8/2-7, Table 1). $\left(+\frac{dH_2O}{dt}\right)$ and Eq. (32'):

$$k_{sh-i}' = \left(+\frac{dH_2O}{dt}\right)/\alpha/\left(P_{CO2}P_{H2} - P_{CO2}^e P_{H2}^e\right) \quad \text{.... (32')}$$

The obtained k'_{sh-i} is expressed as a function of temperature (Eq. (33)) and the activation energy is about 117 kJ. The detail of calculation results in comparison with the observation is shown in later (**Fig. 9**)

$$k_{sh-i}'\left(\frac{cm^3-bed}{s\cdot mol}\right) = 107\times10^{+9}\exp\left(\frac{-117\,430}{RT}\right) \quad \text{..... (33)}$$

The difference of equation is in the term of driving force; $\left(P_{CO2}P_{H2} - P_{CO2}^e P_{H2}^e\right)$. Usually, it may describe like ($P_{CO2}P_{H2} - P_{CO}P_{H2O}/K_W$), in which K_W ($=P_{CO2}P_{H2}/P_{CO}/P_{H2O}$) is an equilibrium constant of WGSR. Actually, K_W must be written as $K_{sh} = P_{CO2}^e P_{H2}^e / P_{CO}^e / P_{H2O}^e$ in order to avoid the confusion with the gases ratio; $K_{sh} = P_{CO2}P_{H2}/P_{CO}/P_{H2O}$). Here, equilibrium constant and gas ratio for inverse WGSR are expressed as $K_{sh-i} = P_{CO}^e P_{H2O}^e / P_{CO2}^e / P_{H2}^e$ and $K_{exp-i} = P_{CO}P_{H2O}/P_{CO2}/P_{H2}$, respectively.

Especially, as mentioned above, the carbon and oxygen

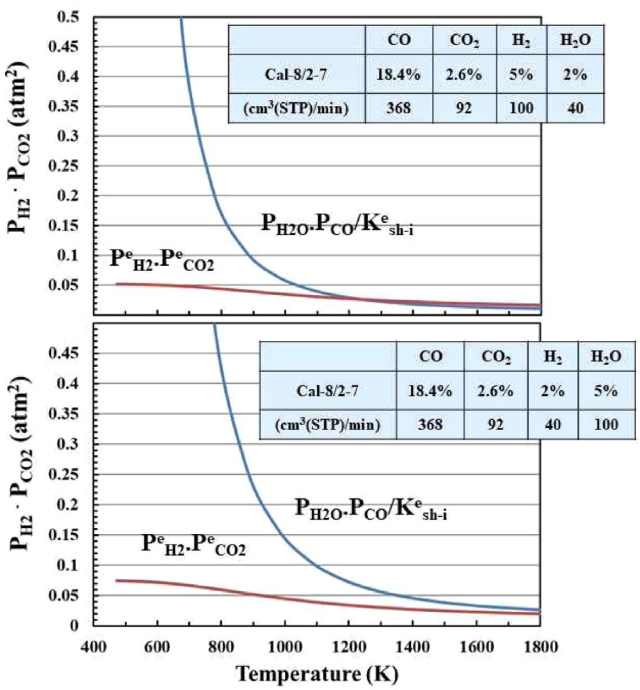

Fig. 6. Comparison of equilibrium composition ($P^e_{H2}P^e_{CO2}$) and conventional equilibrium composition ($P_{H2O}P_{CO}/K^e_{sh-i}$). (Online version in color.)

© 2019 ISIJ

balances are always changed in BF and the WGSR should be considered for the change of the equilibrium condition ($K^e_{sh} = P^e_{CO2}P^e_{H2} / P^e_{CO} / P^e_{H2O}$).

In this study, equilibrium gas flow rates (cm^3(STP)/min), $[H_2]_e$, $[H_2O]_e$. $[CO]_e$, $[CO_2]_e$ were obtained by the calculation method shown in APPENDIX.

As an argon flow rate $[Ar]_0$ is not change before and after reaction, total flow rate, TF can be expressed by Eq. (34).

$$\mathrm{TF} = [\mathrm{Ar}]_0 + [\mathrm{H_2}]_e + [\mathrm{H_2O}]_e + [\mathrm{CO}]_e + [\mathrm{CO_2}]_e \quad \text{... (34)}$$

Then, equilibrium partial pressures can be expressed by Eqs. (35), (36), (37) and (38).

$$P^e_{CO} = \frac{[CO]_e}{TF} \quad \text{..... (35)}$$

$$P^e_{CO2} = \frac{[CO_2]_e}{TF} \quad \text{..... (36)}$$

$$P^e_{H2} = \frac{[H_2]_e}{TF} \quad \text{..... (37)}$$

$$P^e_{H2O} = \frac{[H_2O]_e}{TF} \quad \text{..... (38)}$$

Figure 6 shows the comparison between $P^e_{CO2}P^e_{H2}$ and $P_{H2O}P_{CO} / K^e_{sh-i}$. It is a mater off course, $P^e_{CO2}P^e_{H2}$ is different from $P_{H2O}P_{CO} / K^e_{sh-i}$ and is the same as $P^e_{CO}P^e_{H2O} / K^e_{sh-i}$, when $K^e_{sh-i} = P^e_{CO}P^e_{H2O} / P^e_{CO2} / P^e_{H2}$ is correctly defined. However, the description is sometime omitted as $K^e_{sh-i} = P_{CO}P_{H2O}/P_{CO2}P_{H2}$ for equilibrium constant, so that some confusion may occur from the neglection. The differences between $P^e_{CO2}P^e_{H2}$ and $P_{H2O}P_{CO} / K^e_{sh-i}$ was examined with different initial values as shown in Fig. 6. The difference between $P^e_{CO2}P^e_{H2}$ and $P_{H2O}P_{CO} / K^e_{sh-i}$ is quite large in lower temperature region and become small with increasing temperature.

In the present study, the terms except driving force ($\beta_1 \cdot k'_w$, $\beta_2 \cdot k'_w$, $k'[a_o]$, $\alpha \cdot k'_{sh-i}$) were compared in **Fig. 7**. The activation energy for Ishigaki, *et al.* was lowest and about 32 kJ. On the other hand, the activation energy for Murayama, *et al.* is about 52 kJ, where reduction degree of iron oxide (F) was assumed as unity. When it was assumed that the F changed from 500 K (F=0.01) to 1 500 K (F=1.0), the temperature dependence was increased and was not linear to temperature as shown by short broken line in Fig. 7. The activation energy for Grabke, *et al.* was highest and about 124 kJ. The activation energy for the present study was about 117 kJ, which was close value to Grabke.

3.2. Rate Equation of Gasification Reaction

Y. Kashiwaya, *et al.*[15] have presented the Langmuir-Hinshelwood (L-H) type rate equation for the gasification reaction of coke, in which the crystallinity of graphite structure in coke was taking into account for the rate equation. The equations are expressed separately for the graphite structure and the amorphous structure. Eqs. (39) and (40) show the total rate equation of gasification including Boudouard reaction and water gas reaction I and II for crystallized (graphite) carbon ($k_{W,C}[s^{-1}]$) and amorphous carbon ($k_{W,a}[s^{-1}]$), respectively.

$$k_{W,C}[s^{-1}] = \frac{(k_{1,c-B}P_{CO2} + k_{1,c-W1}P_{H2O})(1 + k_{1,W2})}{1 + k_2P_{CO} + k_3P_{CO2} + k_4P_{H2} + k_5P_{H2O}} \quad \text{... (39)}$$

$$k_{W,a}[s^{-1}] = \frac{(k_{1,a-B}P_{CO2} + k_{1,a-W1}P_{H2O})(1 + k_{1,W2})}{1 + k_2P_{CO} + k_3P_{CO2} + k_4P_{H2} + k_5P_{H2O}} \quad \text{... (40)}$$

where $k_{1,c-B}$ and $k_{1,a-B}$ are rate constants of Boudouard reaction for crystallized carbon and amorphous carbon, respectively. $k_{1,c-W1}$ and $k_{1,a-W1}$ are rate constants of Water gas reaction I. k_{1-W2} is the rate constant of Water gas reaction II. In addition, the rate constants from k_2 to k_5 are the terms of the respective gas adsorption for CO, CO_2, H_2 and H_2O, respectively. The temperature dependence of these rate constants are Eqs. (41)–(49).

$$k_{1,C-B} = \exp\left(9.49 - \frac{24\,200}{T}\right) \quad \text{..... (41)}$$

$$k_{1,a-B} = \exp\left(4.19 - \frac{13\,400}{T}\right) \quad \text{..... (42)}$$

$$k_{1,C-W1} = \exp\left(17.46 - \frac{33\,080}{T}\right) \quad \text{..... (43)}$$

$$k_{1,a-W1} = \exp\left(6.26 - \frac{14\,040}{T}\right) \quad \text{..... (44)}$$

$$k_{1,W2} = \exp\left(-5.41 + \frac{5\,360}{T}\right) \quad \text{..... (45)}$$

$$k_2 = \exp\left(-17.7 + \frac{27\,700}{T}\right) \quad \text{..... (46)}$$

$$k_3 = \exp\left(-1.59 + \frac{5\,680}{T}\right) \quad \text{..... (47)}$$

$$k_4 = \exp\left(-1.14 + \frac{8\,460}{T}\right) \quad \text{..... (48)}$$

$$k_5 = \exp\left(1.86 + \frac{278}{T}\right) \quad \text{..... (49)}$$

The mass fraction of crystallized carbon and amorphous carbon are expressed as N_c and N_a, respectively, and the initial mass of fixed carbon is W_g. The total rate of gasification R_W is expressed by Eq. (50) in moles per second per bed, where N_B means the number of bed divided.

$$R_W\left[mol \cdot s^{-1} \cdot (cm^3 - bed)^{-1}\right] = \left(N_c k_{W.C} + N_a k_{W,a}\right) \cdot \frac{W_g}{12N_B} \quad \text{... (50)}$$

According to elevated temperature, Kashiwaya has assumed that the amorphous carbon decreased, and crystallized carbon increased[15] and there is no amorphous carbon remained over 1 673 K (1 400°C).

$$Nc(-) = 1.380 \times 10^{-9}(T/°\mathrm{C})^3 - 4.287 \times 10^{-6}(T/°\mathrm{C})^2 + 5.873 \times 10^{-3}(T/°\mathrm{C}) - 2.610 \quad \text{... (51)}$$

$$Na = 1 - Nc \quad (\leqq 1\,673\ \mathrm{K}(1\,400°\mathrm{C})) \quad \text{..... (52)}$$

$$Nc = 1,\ Na = 0 \quad (> 1\,673\ \mathrm{K}(1\,400°\mathrm{C})) \quad \text{..... (53)}$$

In the case of graphite crucible, it was assumed that there is no amorphous carbon (Nc=1, Na=0) from room temperature. Although the actual weight of graphite crucible

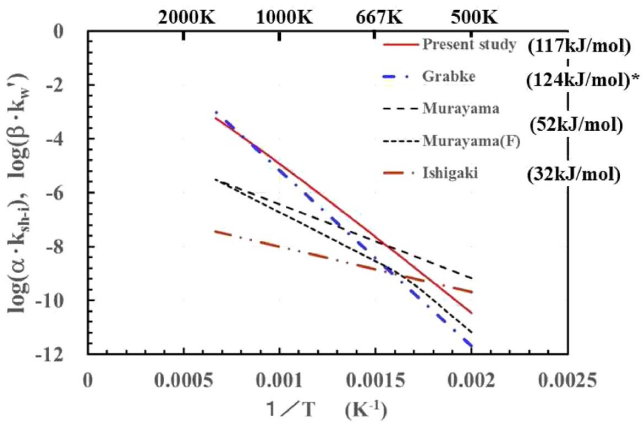

Fig. 7. Comparison of the temperature dependence of apparent rate constants of WGSR for different researchers. (Online version in color.)

© 2019 ISIJ

was more than 100 g, the effective weight for calculation was decided by try and error. Wg for graphite crucible was assumed to be 8 g for Zone 1 and 17 g for Zone 1+2+3 (Table 1), because the reaction of graphite crucible occurs only at the inner surface.

The Eqs. (39) and (40) are divided into the respective rate equations for Boudouard reaction, Water gas reaction I and II, respectively.

Boudouard reaction for crystalline carbon and amorphous carbon:

$$k_{BC}[s^{-1}] = \frac{k_{1,c-B}P_{CO2}}{1+k_2P_{CO}+k_3P_{CO2}+k_4P_{H2}+k_5P_{H2O}} \quad \text{... (54)}$$

$$k_{Ba}[s^{-1}] = \frac{k_{1,a-B}P_{CO2}}{1+k_2P_{CO}+k_3P_{CO2}+k_4P_{H2}+k_5P_{H2O}} \quad \text{... (55)}$$

Water gas reaction I for crystalline carbon and amorphous carbon:

$$k_{W1C}[s^{-1}] = \frac{k_{1,c-W1}P_{H2O}}{1+k_2P_{CO}+k_3P_{CO2}+k_4P_{H2}+k_5P_{H2O}} \quad \text{... (56)}$$

$$k_{W1a}[s^{-1}] = \frac{k_{1,a-W1}P_{H2O}}{1+k_2P_{CO}+k_3P_{CO2}+k_4P_{H2}+k_5P_{H2O}} \quad \text{... (57)}$$

Water gas reaction II for crystalline carbon and amorphous carbon:

$$k_{W2C}[s^{-1}] = \frac{\left(k_{1,c-B}P_{CO2}+k_{1,c-W1}P_{H2O}\right)\left(k_{1,W2}\right)}{1+k_2P_{CO}+k_3P_{CO2}+k_4P_{H2}+k_5P_{H2O}} \quad \text{..... (58)}$$

$$k_{W2a}[s^{-1}] = \frac{\left(k_{1,c-B}P_{CO2}+k_{1,c-W1}P_{H2O}\right)\left(k_{1,W2}\right)}{1+k_2P_{CO}+k_3P_{CO2}+k_4P_{H2}+k_5P_{H2O}} \quad \text{..... (59)}$$

$k_{W.C}$ and $k_{W,a}$ are expressed for the summation of three kinds of gasification reactions as shown by Eqs. (60) and (61).

$$k_{W.C} = k_{B.C} + k_{W1.C} + k_{W2.C} \quad \text{..... (60)}$$

$$k_{W.a} = k_{B.a} + k_{W1.a} + k_{W2.a} \quad \text{..... (61)}$$

Finally, apparent rate of gasification reaction (total beds) can be expressed as Eq. (62).

$$RCS_{cal}\left[mg \cdot min^{-1}\right] = \left(N_c k_{W.C} + N_a k_{W,a}\right) \cdot 60 \cdot W_g \cdot 1\,000 \quad \text{... (62)}$$

And the respective gasification reactions are estimated as follows:

$$K_B\left[mg \cdot min^{-1}\right] = \left(N_c k_{B.C} + N_a k_{B,a}\right) \cdot 60 \cdot W_g \cdot 1\,000 \quad \text{..... (63)}$$

$$K_{W1}\left[mg \cdot min^{-1}\right] = \left(N_c k_{W1.C} + N_a k_{W1,a}\right) \cdot 60 \cdot W_g \cdot 1\,000 \quad \text{... (64)}$$

$$K_{W2}\left[mg \cdot min^{-1}\right] = \left(N_c k_{W2.C} + N_a k_{W2,a}\right) \cdot 60 \cdot W_g \cdot 1\,000 \quad \text{... (65)}$$

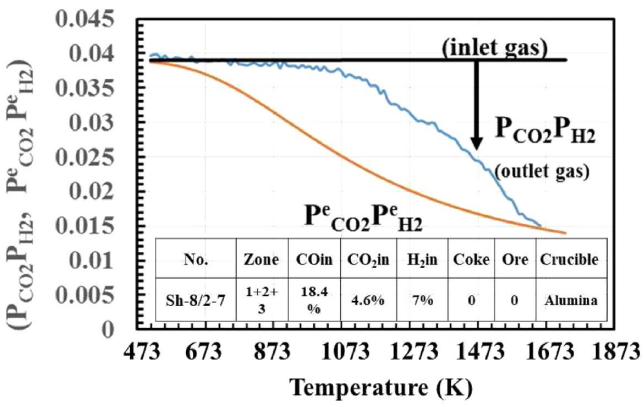

Fig. 8. Change in the product of $P_{CO2}P_{H2}$ by WGSR and the calculated $P^e_{CO2}P^e_{H2}$ in equilibrium. (Online version in color.)

4. Results and Discussions

4.1. Calculation Results of Water Gas Shift Reaction (WGSR)

The result of gas composition change, which obtained by WGSR, is shown in **Fig. 8**. As mentioned above, the crucible used is shown in Fig. 4 and the reaction gas condition is shown in Table 1.

The gas composition in outlet gas, which is shown as $P_{CO2}P_{H2}$, decreased from the initial level with the increasing temperature, which means that the rate of WGSR is increasing with the increasing temperature. Around 1 573 K (1 300°C), the value of $P_{CO2}P_{H2}$ is almost the same as the equilibrium value $P^e_{CO2}P^e_{H2}$. In addition, it was found that the WGSR start to occur from 1 073 K (800°C) in the present experimental condition.

Figure 9 shows the change of partial pressures of respect gases (H_2, H_2O, CO and CO_2) in experiment and the calculated partial pressures. The detail of calculation method of partial pressures was shown in APPENDIX A2. According to the inverse WGSR shown by Eq. (6'), the reaction gases, CO_2 and H_2 decreased from initial gas level, and the product

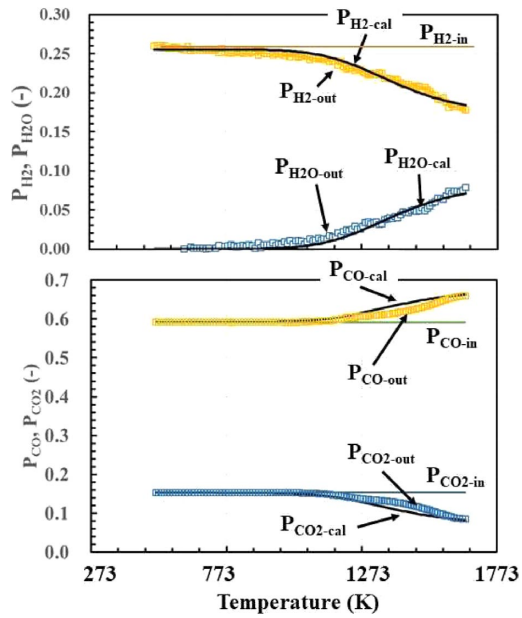

Fig. 9. Variation of partial pressure of reaction gases before and after experiment, and the calculated partial pressures. (Online version in color.)

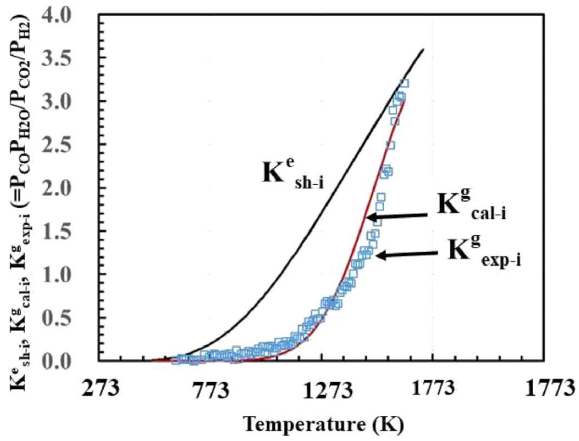

Fig. 10. Calculated result of gas ratio ($K^g_{cal\text{-}i}$) of inverse WSGR in comparison with the gas ratio of experiment ($K^g_{exp\text{-}i}$) and the equilibrium constant ($K^e_{sh\text{-}i}$). (Online version in color.)

© 2019 ISIJ

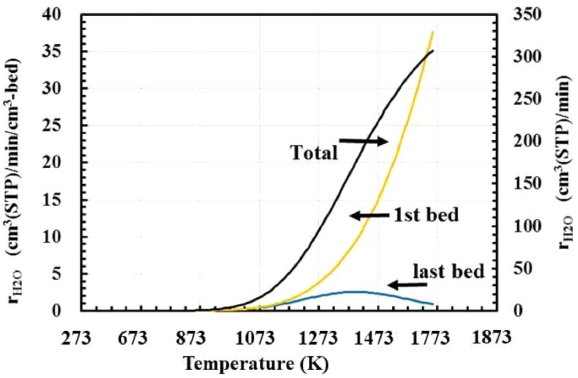

Fig. 11. Calculated results of the total WGSR in comparison with the ones at 1st bed and last (80th) bed. (Online version in color.)

gases, CO and H_2O increased. The calculated results, which are shown by solid lines, are excellent agreement with the observations.

The equilibrium gas constant of inverse WGSR (Eq. (6-a)) can be written as Eq. (66).

$$K^{e}_{sh-i} = \frac{P^{e}_{CO} P^{e}_{H2O}}{P^{e}_{CO2} P^{e}_{H2}} \quad \text{..... (66)}$$

Also, the calculated gas ratio of inverse WGSR is expressed as Eq. (67).

$$K^{g}_{cal-i} = \frac{P_{CO-cal} P_{H2O-cal}}{P_{CO2-cal} P_{H2-cal}} \quad \text{..... (67)}$$

The experimental gas ratio of inverse WGSR is expressed as Eq. (68).

$$K^{g}_{exp-i} = \frac{P_{CO-out} P_{H2O-out}}{P_{CO2-out} P_{H2-out}} \quad \text{..... (68)}$$

The calculated K^{e}_{sh-i}, and K^{g}_{cal-i} are compared with K^{g}_{exp-i} in **Fig. 10**.

In Fig. 10, the calculated results (K^{g}_{cal-i}) of inverse WSGR is compared with the equilibrium gas constant (K^{e}_{sh-i}) and the gas ratio of experiment (K^{g}_{exp-i}). The experimental gas ratio of inverse WGSR is always lower than that of equilibrium gas constant (K^{e}_{sh-i}). The calculated result (K^{g}_{cal-i}) is in excellent agreement with the observation (K^{g}_{exp-i}). As shown in Fig. 8, the gas ratio of experiment (K^{g}_{exp-i}) is approaching to the equilibrium value (K^{e}_{sh-i}) with the increase of temperature and become almost the same around 1 573 K (1 300°C).

Figure 11 shows the calculated results of WGSR in the fixed bed. Total rate of WGSR increases exponentially with the increasing temperature until 1 373 K (1 100°C), and then the increasing rate decreases after 1 373 K. In this case, the bed was divided into 80. The rate of WGSR at 1st bed is exponentially increased with increasing temperature, because the reaction gas is always fresh (the same as the initial composition). According to go upper bed, the composition of input gas to the divided bed is changing and close to an equilibrium. Finally, the rate of WGSR at the last bed is very low as shown in Fig. 11. From these results, it was found that the distribution of WGSR in the total beds is largely changed and the gas composition in the upper bed is almost close to the equilibrium.

4.2. Calculation Results of Gasification Reaction

4.2.1. Gasification Reaction without WGSR (Ar–CO–CO_2 System)

Figure 12 shows the calculation results of gasification reaction in Zone 1 and Zone 1+2+3 under different gas composition (CO/CO_2=9/1 and 8/2).

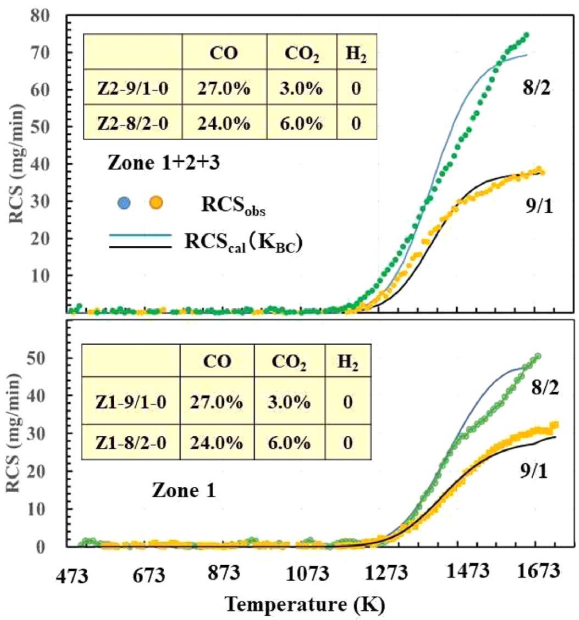

Fig. 12. Calculated results of gasification reaction in Zone 1 and Zone 1+2+3 under Ar–CO–CO_2 system. (Online version in color.)

In the case of Zone 1, the calculation results for 9/1 and 8/2 are in good agreement with the observations. In the higher temperature range, the calculation results could not be fitted completely with the observation, because the structure of coke bed might change from the increasing gasification degree, which were considered about 32% for 9/1 and about 50% for 8/2. In addition, since the crucible used was Fig. 3(c), the alumina balls instead of pellets were relatively easy to move during experiment. The movement of alumina balls will affect on the gas stream strongly, so that the result of gasification might scatter among different experiment. Furthermore, the existence of ash layer formed on the surface of coke will generally inhibit the rate of gasification, however, the ash layer is easy to fall away by some small vibration such as the movement of alumina balls.

In the case of Zone 1+2+3, the calculation results were relatively difficult to fit the observations. The cause might be in the experimental results at Zone 2, because the reaction surface in Zone 2 is only inner surface of graphite crucible and is strongly affected by the actual gas flow which is controlled by the structure of bed, significantly. However, in spite of these difficulties, the calculation results are in good agreement the observation approximately.

As a result, it was concluded that the total gasification reaction can be calculated within an experimental error.

4.2.2. Gasification Reaction with WGSR in Ar–CO–CO_2–H_2 System

Figure 13 shows the comparison of the experimental results and the calculation results of gasification rates (K_B, K_{W1} and K_{W2}.) together with WGSR for zone 1 and zone 1+2+3. Total gasification rate is expressed as RCS_{cal} and the observation is expressed as RCS_{obs}. The RCS_{cal} is in good agreement with RCS_{obs} both in Zone 1 and Zone 1+2+3.

Although the difference between RCSobs and RCScal in Zone 1+2+3 increased in the higher temperature rage over 1 473 K, the causes will be resulted from the change of gas stream in high temperature as mentioned above.

In this study, the quantification of reaction rate was performed by gas analysis method as mentioned above. The RCScal can be separated into three kinds of gasification reactions, K_B, K_{W1} and K_{W2}. The gas analysis method for the quantification of the reaction rate has a significant merit on

© 2019 ISIJ

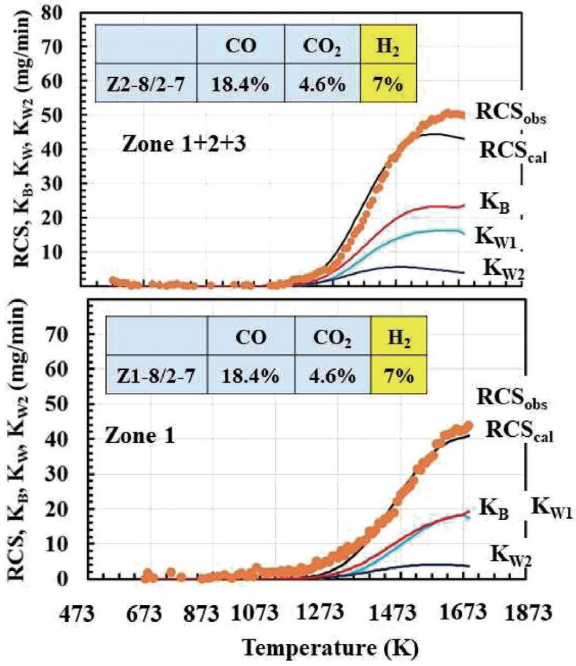

Fig. 13. Calculated results of gasification reaction for zone 1 and zone 1+2+3 under Ar–CO–CO_2–H_2 system.

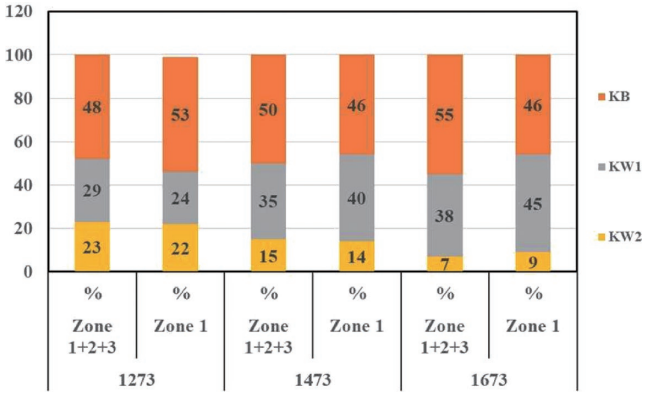

Fig. 14. Comparison of gasification rates (K_B, K_{W1} and K_{W2}) for zone 1 and zone 1+2+3 at different temperatures .

Table 3. Calculated gasification rates among different reactions (RCS_{cal}, K_B, K_{W1} and K_{W2}) at 1 273 K, 1 473 K and 1 673 K in Zone 1 and Zone 1+2+3.

Temp. (K)	Zone		RCS_{cal}	K_B	K_{W1}	K_{W2}
1 273	Zone 1+2+3	mg/min	9.17	4.44	2.66	2.07
		%	100	48	29	23
	Zone 1	mg/min	3.79	2.0	0.94	0.85
		%	100	53	24	22
1 473	Zone 1+2+3	mg/min	38.6	19.4	13.6	5.55
		%	100	50	35	15
	Zone 1	mg/min	25.6	11.6	10.4	3.6
		%	100	46	40	14
1 673	Zone 1+2+3	mg/min	42.2	23.1	15.9	3.18
		%	100	55	38	7
	Zone 1	mg/min	40.4	18.5	18.1	3.8
		%	100	46	45	9

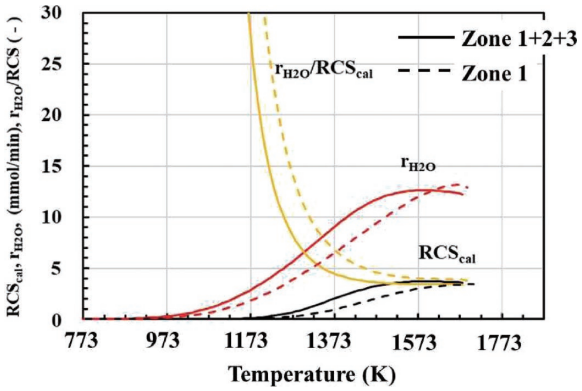

Fig. 15. Comparison of rates of WGSR and gasification reactions for Zone 1 and Zone 1+2+3.

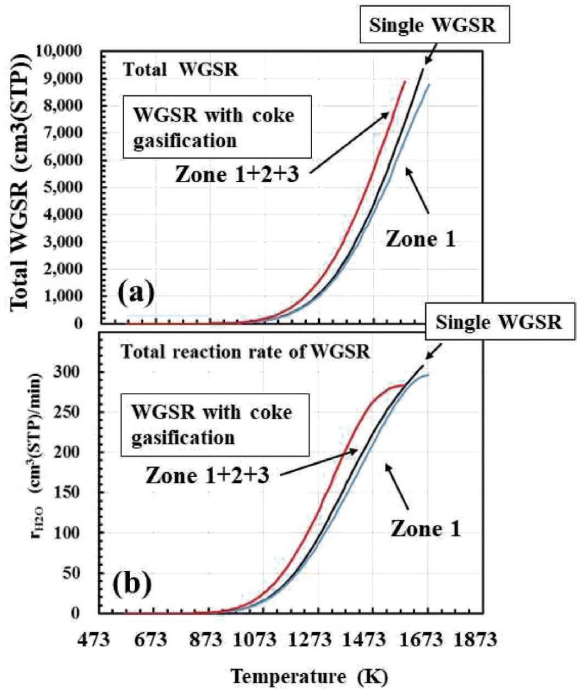

Fig. 19. Comparison of WGSR occurring with gasification reaction in Zone 1, Zone 1+2+3 and single reaction system. (a) the amount of WGSR, (b) the rate of WGSR.

the analysis of reaction system containing hydrogen.

In **Table 3** and **Fig. 14**, the values of gasification rates for Zone 1 and Zone 1+2+3 are shown at the different temperature (1 273 K, 1 473 K and 1 673 K).

Water gas reaction II (K_{W2}) is lowest in comparison with Boudouard reaction (K_B) and water gas reaction I (K_{W1}). The amount of K_{W2} decreases with the increase of temperature both in Zone 1 and Zone 1+2+3.

When the values of K_{W2} in Zone 1 and Zone 1+2+3 are compared, the difference is not so large in spite of the large difference of volume, which means that the gas composition change in Zone 1 is significant and the inlet gas composition to the upper zone (Zones 2 and 3) has a little difference with the equilibrium composition.

The rate of Boudouard reaction (K_B) is largest in comparison with the other reactions (K_{W1} and K_{W2}). K_B was changed by temperature so as to 48%→50%→55% in Zone 1+2+3 and 53%→46%→46% in Zone 1.

On the other hand, Water gas reaction I (K_{W1}) increased with temperature and is 29%→35→38% in zone 1+2+3 and is 24%→40%→45% in Zone 1. From these results, it is considered that the variation of gasification rates (K_B, K_{W1} and K_{W2}) is complicated and is changed with the tempera-

© 2019 ISIJ

ture and the locations occurring.

4.3. Effect of WGSR on Gasification Reaction

Figure 15 shows the ratio of WGSR to gasification reaction (r_{H2O}/RCS_{cal}) and respective rates of WGSR and gasification reactions for Zone 1 and Zone 1+2+3. Both terms in the ratio, r_{H2O}/RCS_{cal} are in the unit of mmol/min. The extent of the ratio means the tendency of the gas composition change through WGSR and gasification reaction.

The r_{H2O} of WGSR means the formation of H_2O and CO gases, and the vanishing of CO_2 and H_2 gases.

On the other hand, since RCScal includes three kinds of reaction (K_B, K_{W1} and K_{W2}), it is quite difficult to understand the behaviors. However, in the present study, it was succeeded to estimate three kinds of reaction (K_B, K_{W1} and K_{W2}) separately. As shown in Fig. 14 and Table 3, the proportion of water gas reactions I and II (K_{W1} and K_{W2}), which are corresponding to the consumption of H_2O, is about 50% for the total gasification reaction. The ratio, r_{H2O}/RCS_{cal} is very high (> 5) in low temperature range below 1 423 K for Zone 1 and 1 323 K for Zone 1+2+3, which means the formation of H_2O through WGSR is significant comparing to the consumption of H_2O by Water gas reactions I (K_{W1}) and II (K_{W2}). Since the proportion of K_{W1} and K_{W2} is about 50% to total gasification reactions, the value of ratio, r_{H2O}/RCS_{cal} means about twice in terms of the consumption of H_2O. In high temperature region over 1 473 K, the ratios, r_{H2O}/RCS_{cal} become almost constant and is about less than 4 for Zone 1 and about 3 for Zone 1+2+3, which means that WGSR and gasification reaction are balanced in some magnitude in high temperature range more than 1 473 K.

The value of r_{H2O} over 1 573 K for Zone 1, which is expressed in broken line in Fig. 15, was higher than that of Zone 1+2+3. Since it is strange result, the exprerimental conditions were checked again and the heating-up rates in both experiments between Zone 1 and Zone 1+2+3 were compared. Then, the heating-up rate over 1 573 K for Zone 1 was 12 K/min which was higher than the desired condition (10 K/min). It is considered that although the rate of WGSR, r_{H2O}, was higher, the ratio $r_{H2O}/RCScal$, is not changed and moved smoosely with temperature. The r_{H2O} and RCScal are reasonably changed with temperature.

Figure 16 shows the comparison of the variation of partial pressure of gases between calculation and observation in which WGSR and gasification reactions occur together. The calculation results are in excellent agreement with the observation. It is important to note that not only the apparent gasification rate but also the gas composition change should be fit in the kinetic analysis for the reaction system in CO–CO_2–H_2–H_2O. According to the elevated temperature, CO_2 and H_2 in the inlet gas decreased and CO and H_2O increased from initial level apparently. It is quite interesting to note the variation of H_2O. The partial pressure of H_2O gradually increased from low temperature and showed maximum at around 1 373 K, then, decreased and became almost zero over 1 573 K. This behavior of H_2O was strongly connected with the variation of ratio, r_{H2O}/RCS_{cal} as shown in Fig. 15. In the low temperature region below 1 373 K, WGSR is dominant, and in high temperature region, the gasification reaction become dominant, and H_2O formed by WGSR will be consumed significantly as temperature increases.

Figure 17 shows the variations of gas ratio of WGSR, K^g_{exp-i} and K^g_{cal-i}, in comparison with the equilibrium con-

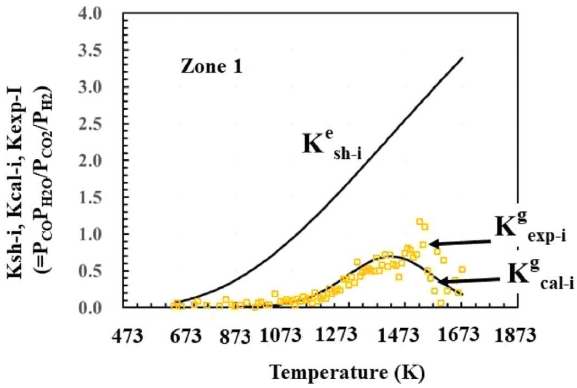

Fig. 17. Comparison of gas ratio of WSGR among K^g_{exp-i}, K^g_{cal-i} and the equilibrium constant K^e_{sh-i}. (Online version in color.)

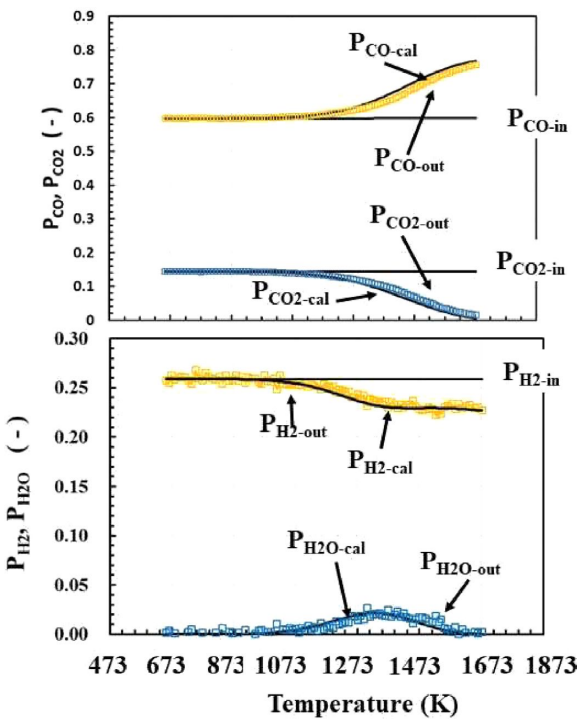

Fig. 16. Comparison of the variation of partial pressure of gases between calculation and observation occurring WGSR and gasification reactions. (Online version in color.)

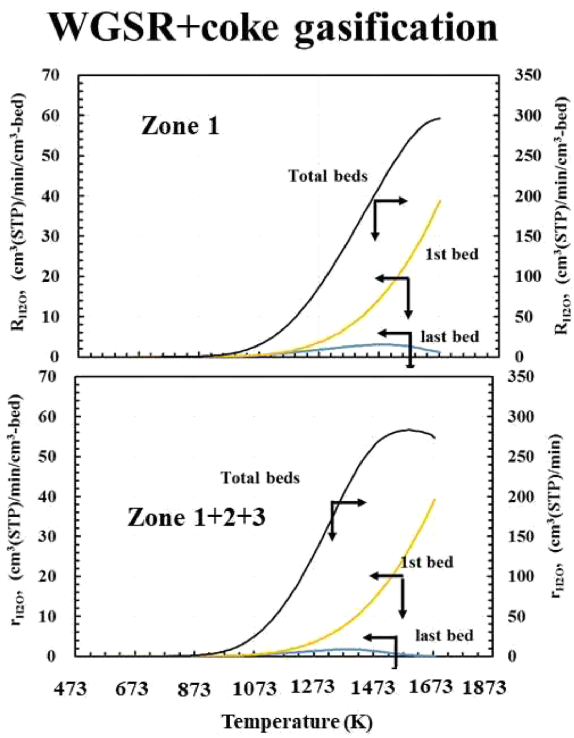

Fig. 18. Comparison of the rates of WGSR in first bed, last bed and total bed together with gasification reaction. (Online version in color.)

© 2019 ISIJ

stant K^{e}_{sh-i}. When these gas ratios were compared with the one of single WGSR (Fig. 10), it was found that the behavior of K^{g}_{cal-i} and K^{g}_{exp-i} is clearly affected by gasification reaction in high temperature region over 1 373 K. The rate of Water gas reaction I increases with the increasing temperature exponentially, in which the existing H_2O is consumed significantly.

Figures 18(a) and 18(b) show the rate of WGSR at 1st bed, last bed and total beds in Zone 1 and Zone 1+2+3, respectively. The rate of WGSR at 1st bed is highest and the one at last bed is lowest, because the inlet gas composition of each bed is approaching to the equilibrium according to go the upper bed. Furthermore, in high temperature range over 1 573 K, the rate of WGSR become almost zero, which means the both of CO_2 and H_2O will be almost consumed by gasification reaction around last bed in Zone 1+2+3.

The difference between Zone 1 and Zone 1+2+3 is not so large as shown in Fig. 15 (solid line and broken line). Since the volume of reaction is larger in Zone 1+2+3, WGSR around last bed become almost zero in higher temperature, and the total rate of WGSR become flat as shown in Fig. 18.

Figure 19 shows the comparison of WGSR occurring with gasification reaction in Zone 1, Zone 1+2+3 and single reaction system ((a) the amount of WGSR, (b) the rate of WGSR). As mentioned above, the reaction volume of Zone 1+2+3 is about 4 times larger than that of Zone 1. While the reaction volume of single WGSR is the same as Zone 1+2+3. When the rate of WGSR in Zone 1+2+3 is compared with single WGSR system, the amount of WGSR together with gasification reaction is about 1.5 times larger than that of single WGSR. And the single WGSR is almost the same with the rate of WGSR in Zone 1 in spite of large difference of reaction volume.

5. Conclusions

The Water gas shift reaction (WGSR) was examined experimentally and kinetic analysis was performed with and without gasification reaction. The quantification of reaction rates was carried out by gas analysis method. Several kind of crucibles were developed for determining the respective reaction rates occurring in different position.

(1) The rate equation of invers WGSR was decided as

$$R_{sh-i} = -\frac{dCO_2}{dt} = +\frac{dH_2O}{dt} = r_{H2O}\left(\frac{mol}{s\cdot cm^3-bed}\right)$$
$$= Ak_{sh-i}\left(C_{CO2}C_{H2} - C^{e}_{CO2}C^{e}_{H2}\right)$$

where the rate constant in the alumina crucible was obtained as

$$k'_{sh-i}\left(\frac{cm^3-bed}{s\cdot mol}\right) = 107\times10^{+9}\exp\left(\frac{-117\,430}{RT}\right)$$

(2) The single WGSR is closed to the equilibrium state over 1 573 K.

(3) Calculation of gasification reaction (K_B, Boudouard reaction) in Zone 1 and Zone 1+2+3 were in excellent agreement with the observation under CO–CO_2 system (without Hydrogen).

(4) When H_2 was added to the reaction gases, Water gas reaction I (K_{W1}) and II (K_{W2}) in addition to K_B were considered to the calculation and the total gasification reaction RCS_{cal} ($=K_B+K_{W1}+K_{W2}$) was in excellent agreement with the observation, which meant that the gasification reactions could be separated into K_B, K_{W1} and K_{W2}.

(5) The proportion of K_B was about 50% which increased from 48% (1 273 K) to 55% (1 673 K) in Zone 1+2+3. On the other hand, the proportion of K_{W2} was lowest and decreased from 23% (1 273 K) to 7% (1 673 K). The proportion of K_{W1} increased from 29% (1 273 K) to 38% (1 673 K) in Zone 1+2+3.

(6) The ratio of WGSR to gasification reaction (r_{H2O}/RCS_{cal}) was high (> 5) in low temperature range below 1 153 K for Zone 1 and 1 323 K for Zone 1+2+3, which means the formation of H_2O through WGSR is significant comparing to the consumption of H_2O by Water gas reactions I (K_{W1}) and II (K_{W2}). In high temperature region over 1 373 K, the ratios, r_{H2O}/RCS_{cal} become almost constant and is about less than 4 for Zone 1 and about 3 for Zone 1+2+3.

(7) The variations of gases partial pressure obtained by calculation were in excellent agreement with observation under existence of WGSR and gasification reactions. The variation of H_2O showed maximum around 1 373 K and then decreased in the higher temperature region. This behavior was resulted from magnitude relationship between WGSR and gasification reaction.

(8) The amount of WGSR occurring with gasification reaction was about 1.5 times larger than that of single WGSR.

Nomenclature

u: Linear velocity (cm/s, at STP),
ε: Void fraction (–),
C: Concentration of gas (mol/cm^3),
V_B: Volume of bed (cm^3-bed),
N_B: Number of bed (–)
N_c, N_a: Mass fraction of crystallized carbon and amorphous carbon (–)
t: time (s),
W_0: Initial reducible oxygen (g-O/cm^3-bed),
W_g: Initial mass of fixed carbon in coke (g)
z: Height of bed (cm),
G: amount of gasification (g-C/cm^3-bed),
F: Fraction of reduction (–)
R_{H2}, R_{CO}: Rate of reduction by H_2 and CO (mol/s/cm^3-bed)
R_B: Rate of gasification (Boudouard reaction) (mol/s/cm^3-bed)
R_{BC}: Rate of gasification (Boudouard reaction) of coke (mol/s/cm^3-bed)
R_{BG}: Rate of gasification (Boudouard reaction) of graphite (mol/s/cm^3-bed)
R_W: Rate of water gas reaction I (mol/s/cm^3-bed)
R_{WC}: Rate of water gas reaction I of coke (mol/s/cm^3-bed)
R_{WG}: Rate of water gas reaction I of graphite (mol/s/cm^3-bed)
R_{W2}: Rate of water gas reaction II (mol/s/cm^3-bed)
R_{W2C}: Rate of water gas reaction II of coke (mol/s/cm^3-bed)
R_{W2G}: Rate of water gas reaction II of graphite (mol/s/cm^3-bed)
$R_{sh\text{-}i}$: Rate of inverse water gas shift reaction (mol/s/cm^3-bed)
$k_{W.C}$: Rate of total gasification of crystallized carbon (1/s)
$k_{B.C}$: Rates of Boubouard reaction of crystallized carbon (1/s)
$k_{W1.C}$: Rates of Water gas reaction I of crystallized carbon (1/s)
$k_{W2.C}$: Rates of Water gas reaction II of crystallized carbon (1/s)
$k_{W.a}$: Rate of total gasification of amorphous carbon (1/s)
$k_{B.a}$: Rates of Boudouard reaction I of amorphous carbon (1/s)
$k_{W1.a}$: Rates of Water gas reaction I of amorphous carbon (1/s)
$k_{W2.a}$: Rates of Water gas reaction II of amorphous carbon (1/s)
K_B: Rate of Boudouard reaction (mg/min)
K_{W1}: Rate of Water gas reaction I (mg/min)
K_{W2}: Rate of Water gas reaction II (mg/min)
K^{e}_{sh-i}: Equilibrium gas constant of inverse WGSR (–)
K^{g}_{X}: Ratio of gas partial pressure of X(=*cal-i, exp-i*) (–)

© 2019 ISIJ

REFERENCES

1) K. Ishii, N. Kasai, Y. Kashiwaya and S. Kondo: *Tetsu-to-Hagané*, **73** (1987), 1519 (in Japanese).
2) K. Ishii, Y. Kashiwaya, H. Yamaguchi and S. Kondo: *Tetsu-to-Hagané*, **72** (1986), 2202 (in Japanese).
3) Y. Kashiwaya and M. Hasegawa: *ISIJ Int.*, **52** (2012), 1513.
4) J. Vahdati Khaki, Y. Kashiwaya and K. Ishii: *Ironmaking Steelmaking*, **21** (1994), 56.
5) Y. Kashiwaya, H. Kadoya, M. Sakawa, T. Konno and K. Ishii: *Tetsu-to-Hagané*, **82** (1996), 653 (in Japanese).
6) L. Gradisher, B. Dutcher and M. Fan: *Appl. Energy*, **139** (2015), 335.
7) R. J. B. Smith, M. Loganatham and M. S. Shantha: *Int. J. Chem. React. Eng.*, **8** (2010), R4.
8) T. L. LeValleya, A. R. Richarda and M. Fan: *Int. J. Hydrog. Energy*, **39** (2014), 16983.
9) A. Kemppainen, T. Alatarvas, M. Iljana, J. Haapakangas, O. Mattila, T. Paananen and T. Fabritius:: *ISIJ Int.*, **54** (2014), 801.
10) T. Murayama, K. Higashi, K. Imanishi and Y. Ono: *Tetsu-to-Hagané*, **78** (1992), 998 (in Japanese).
11) M. Ishigaki, R. Takahashi and A. Takahashi: *Bull. Res. Inst. Miner. Dress. Metall. Tohoku Univ.*, **38** (1982), 36.
12) P. J. Meschter and H. J. Grabke: *Metall. Trans. B*, **10** (1979), 323.
13) Y. Kashiwaya and K. Ishii: *Tetsu-to-Hagané*, **76** (1990), 1254 (in Japanese).
14) Y. Kashiwaya and K. Ishii: *Tetsu-to-Hagané*, **79** (1993), 1305 (in Japanese).
15) Y. Kashiwaya and K. Ishii: *Tetsu-to-Hagané*, **79** (1993), 1311 (in Japanese).

Appendix

A1: Estimation of Equilibrium Gas Composition

- $$[O]_0 = [CO]_{in} + 2[CO_2]_{in} + [H_2O]_{in} = [CO]_e + 2*[CO_2]_e + [H_2O]_e + [O]_{RDR} \quad \text{.... (A1)}$$
- $$[C]_0 = [CO]_{in} + [CO_2]_{in} = [CO]_e + [CO_2]_e + [C]_{RCS} \quad \text{..... (A2)}$$
- $$[H_2]_0 = [H_2]_{in} + [H_2O]_{in} = [H_2]_e + [H_2O]_e \quad \text{... (A3)}$$

where $[O]_0$, $[C]_0$, $[H_2]_0$ are initial flow rates of oxygen, carbon and hydrogen in the initial gas (cm^3(STP)/min). $[CO]_{in}$, $[CO_2]_{in}$, $[H_2O]_{in}$ are initial flow rates of CO, CO_2 and H_2O. $[CO]_e$, $[CO_2]_e$, $[H_2O]_e$ are the flow rates of CO, CO_2 and H_2O in equilibrium.

$[O]_{RDR}$ and $[C]_{RCS}$ are the oxygen and carbon moved from solid phase to gas phase (cm^3(STP)/min) through reduction reaction and gasification reaction.

In the case of single WGSR analysis, $[O]_{RDR}=0$ and $[C]_{RCS}=0$.

The WGSR is expressed as Eq. (A4) and the equilibrium constant is defined as *Ksh*

$$H_2O + CO = CO_2 + H_2, \quad \text{..... (A4)}$$

A standard Gibbs energy was calibrated with the function of temperature using HSC Chemistry 9 (Outotec).

$$dG^0 / \text{kcal} = -1.09526\times10^{-6}T^2 + 9.96613\times10^{-3}T - 9.56113$$

$$(T : \text{Kelvin})$$

$$K_{sh} = \left([CO_2]_e \cdot [H_2]_e\right) / \left([H_2O]_e \cdot [CO]_e\right) \quad \text{..... (A5)}$$

Quadratic equation about $[H_2]_e$ can be calculated by Eqs. (A6) and (A7).

$$(1-K_{sh})\left([H_2]_e\right)^2 + \left\{K_{sh}\left(2[C]_0 - [O]_0 + 2[H_2]_0\right) + [O]_0 - [C]_0 - [H_2]_0\right\}\left([H_2]_e\right) - K_{sh}[H_2]_0\left(2[C]_0 - [O]_0 + [H_2]_0\right) = 0 \quad \text{..... (A6)}$$

$$a\left([H_2]_e\right)^2 + b\left([H_2]_e\right) + c = 0 \quad \text{..... (A7)}$$

Finally, respect equilibrium gas flow rate can be obtained.

$$[H_2]_e = \frac{-b + \sqrt{\left(b^2 - 4ac\right)}}{2a} \quad \text{..... (A8)}$$

$$[H_2O]_e = [H_2]_0 - [H_2]_e \quad \text{..... (A9)}$$

$$[CO]_e = [C]_0[H_2]_e / \left(K_{sh}[H_2]_0 - K_{sh}[H_2]_e + [H_2]_e\right) \quad \text{..... (A10)}$$

$$[CO_2]_e = [C]_0 - [CO]_e \quad \text{.....(A11)}$$

A2: Calculation Method of Outlet Gas Partial Pressure

The outlet gas flow rate can be calculated by Eqs. (A15)–(A15)

$$[H_2]_{out}\left(\frac{cm^3(STP)}{\text{min}}\right) = [H_2]_{in}\left(\frac{cm^3(STP)}{\text{min}}\right) + \left(-R_{H2} + R_W + 2R_{W2} - R_{sh-i}\right)N_B \cdot V_B \cdot 60 \cdot 22\,414 \quad \text{... (A12)}$$

$$[H_2O]_{out}\left(\frac{cm^3(STP)}{\text{min}}\right) = [H_2O]_{in}\left(\frac{cm^3(STP)}{\text{min}}\right) + \left(R_{H2} - R_W - 2R_{W2} + R_{sh-i}\right)N_B \cdot V_B \cdot 60 \cdot 22\,414 \quad \text{... (A13)}$$

$$[CO]_{out}\left(\frac{cm^3(STP)}{\text{min}}\right) = [CO]_{in}\left(\frac{cm^3(STP)}{\text{min}}\right) + \left(-R_{CO} + 2R_B + R_W + R_{sh-i}\right)N_B \cdot V_B \cdot 60 \cdot 22\,414 \quad \text{... (A15)}$$

$$[CO_2]_{out}\left(\frac{cm^3(STP)}{\text{min}}\right) = [CO_2]_{in}\left(\frac{cm^3(STP)}{\text{min}}\right) + \left(R_{CO} - R_B + R_{W2} - R_{sh-i}\right)N_B \cdot V_B \cdot 60 \cdot 22\,414 \quad \text{... (A16)}$$

The partial pressures of respective gases were calculated by the same way from Eqs. (34) to (38).

© 2019 ISIJ